Scientific Research Publishing

Computational Chemistry, 2024, 12, 1-23
https://www.scirp.org/journal/cc
ISSN Online: 2332-5984
ISSN Print: 2332-5968

Theoretical Investigation on the Stability and Reactivity of Imidazo [1,2-a] Pyridine *N-Acylhydrazone* Derivatives Using Density Functional Theory

Camara Tchambaga Etienne[1*], Sangare Kassoum[2], Dosso Ouehi[1], Ablo Evrard[1,3], Sekou Diomande[2], Souleymane Coulibaly[1*], Siomenan Coulibali[1]

[1]Laboratoire de Constitution et de Réaction de la Matière (LCRM) de l'UFR SSMT, Université Félix Houphouët-Boigny, Abidjan, Côte d'Ivoire
[2]Département des Sciences et Technologies Agro-industrielles (STAgI), UFR Agriculture, ressources halieutiques et agro-industrie (ARHAI), Université de San Pedro, San Pedro, Côte d'Ivoire
[3]Laboratoire des Procédés Industriels de Synthèse, de l'Environnement et des Énergies Nouvelles (LAPISEN), Institut National Polytechnique FélixHouphouët-Boigny, Yamoussoukro, Côte d'Ivoire
Email: *tchambaga01@yahoo.fr, *souleydestras@yahoo.fr

How to cite this paper: Etienne, C.T., Kassoum, S., Ouehi, D., Evrard, A., Diomande, S., Coulibaly, S. and Coulibali, S. (2024) Theoretical Investigation on the Stability and Reactivity of Imidazo [1,2-a] Pyridine *N-Acylhydrazone* Derivatives Using Density Functional Theory. *Computational Chemistry*, **12**, 1-23.
https://doi.org/10.4236/cc.2024.121001

Received: January 2, 2024
Accepted: January 28, 2024
Published: January 31, 2024

Abstract

The reactivity and stability of seventeen (17) imidazo [1,2-a]pyridine *N-acylhydrazone* derivatives were investigated using density functional theory at the B3LYP/6-31+ G (d, p) level. Analysis of the molecular electrostatic potential (MEP) and determination of the dual descriptor revealed that in most cases, the nitrogen atoms of the 6-πelectron conjugation, the oxygen, and the sulfur atom are nucleophilic site. Chemical reactivity of the compounds was assessed through analysis of frontier molecular orbitals (HOMO and LUMO), energy gap ($\Delta\mathcal{E}$), chemical hardness (η), and the softness (S). Consequently, the compound **9e** exhibited the lowest reactivity, least electron donating, and the highest stability. This comprehensive study offers valuable insights into the chemical behavior of these derivatives, crucial for further exploration and potential applications.

Keywords

N-Acylhydrazones, Imidazo [1,2-a] Pyridine, DFT, Molecular Electrostatic Potential, Reactivity, Stability

1. Introduction

In recent years, research interest in *N-acylhydrazones* containing the heterocyclic imidazo [1,2-a] pyridine scafflold has seen remarkable growth [1]-[3]. *N-*

acylhydrazones represent a conjugated system with 6π electrons, provided that the azomethine group adopts the most stable E configuration. This conjugated system can undergo two additional isomerizations, resulting from slow rotation around the N-N and N-CO bonds (**Figure 1**), potentially yielding four distinct conformers. This conformational diversity underscores the importance of understanding the structure and reactivity of these compounds. *N-acylhydrazone* molecules hold significant interest due to their diverse potential applications, including as ligands in asymmetric catalysis, antibacterial agents [4]-[6], antifungals [7], antitumor agents [8]-[10], among others [11]-[13]. In previous study, our team synthesized a series of molecules belonging to this family [14]. The current study aims to theoretically examine the reactivity, stability, and identify nucleophilic/electrophilic attack sites using various quantum chemistry methods to optimize their properties. All simulations were conducted in the gas phase, employing the B3LYP/6-31+G (d, p) level of theory. Reactivity and stability were assessed through the calculation of descriptors such as energy gap ($\Delta\mathcal{E}$), chemical hardness (η), and softness (S). Nucleophilic/electrophilic attack sites were determined via analysis of the molecular electrostatic potential (MEP) map as well as the dual descriptor. This systematic approach will illuminate our understanding of molecular interactions and pave the way for the design and modelling of more effective and targeted compounds for a diverse range of applications.

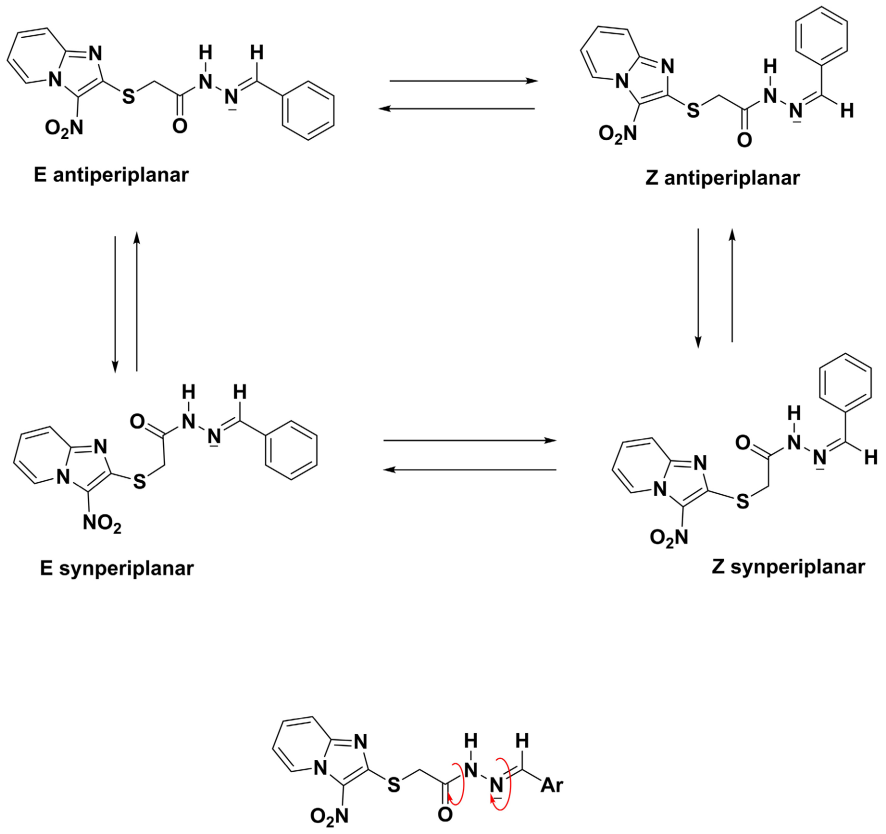

Figure 1. Four possible rotamers of the *N-acylhydrazone* moiety

2. Materials and methods

2.1. Materials

The molecules studied were listed in Table 1.

Table 1. Variations in aromatic (Ar) substituents among studied *N-Acylhydrazone* derivatives: set of the molecular structures.

Compounds	Ar
9a	Phenyl
9b	2-hydroxyphenyl
9c	4-fluorophenyl
9d	4-toluyl
9e	4-nitrophenyl
9f	4-methoxyphenyl
9g	4-hydroxy-3-methyloxyphenyl
9h	4-hydroxyphenyl
9i	4-cyanophenyl
9j	4-*N*,*N*-dimethylaminophenyl
9k	4-chlorophenyl
9m	3,5-dichlorophenyl
9n	4-methylbenzyloxyphenyl
9o	4-methoxybenzyloxyphenyl
9p	benzylthiophenyl
9q	thiophen-2-yl
9r	furan-2-yl

2.2. Computational Details

The computational analysis was conducted utilizing Gaussian 09 software [15], leveraging the density functional theory (DFT) method [16]. The results have been visualized using the GaussView 6 program [17]. DFT was chosen due to its established capability in accurately predicting molecular properties. Specifically, hybrid functional methods like B3LYP, known for their robustness and wide applicability, were employed [18]. The selected level of theory for this investigation was B3LYP/6-31+G(d,p). Each *N-acylhydrazone* molecule underwent rigorous molecular geometry optimization, followed by frequency calculations to verify the stability of the optimized structure. Furthermore, a comprehensive suite of stability and reactivity parameters were computed for in-depth analysis of the molecular properties, providing nuanced insights into the structure and behavior of these compounds.

Reactivity descriptors

1) Electrostatic Potential Surface (EPS) Area

Electrostatic Potential Surfaces (EPS) and its cartography serve as indispensable tools for analyzing and predicting the reactive behavior of molecules. By scrutinizing the EPS surface, one can identify potentially reactive regions through an intuitive colorimetric representation. The color gradient typically progresses as follows: red < orange < yellow < green < cyan < blue [19] [20]. In the electrostatic potential surface, areas with zero potential are depicted in green, negative regions (red and yellow) denote electrophilic attack sites, while positive areas (cyan and blue) signify nucleophilic attack sites. This visual representation facilitates rapid and accurate identification of reactive sites, thereby enhancing our comprehension and predictive capabilities regarding molecular reactions.

This method hinges on Equation (1), defining the EPS as the interaction energy of a proton with the nucleus and electrons of a molecule.

$$V(r)=\sum_{A}^{\text{Nucleus}}\frac{Z_A}{\left|R_A-r\right|}-\int\frac{\rho(r')\mathrm{d}r'}{\left|r'-r\right|} \tag{1}$$

In this equation, Z_A represents the charge of the nucleus A, $\left|R_A-r\right|$, $\left|r'-r\right|$ signify the proton-nucleus and proton-electron distances respectively, while $p(r')$ represents the electron density.

2) Global molecular descriptors

Global descriptors plays are indispensable tools in characterizing molecular properties, offering a comprehensive view of a system's stability and reactivity. Unlike local descriptors, which vary across chemical space, global descriptors maintain a uniform value throughout the system under examination. Their uniformity enables an assessment of the system's response to global perturbations, providing insights into macroscopic properties [21]. Among these descriptors, hardness (η) and softness (S) hold particularly significance. Hardness the first derivative of the chemical potential with respect to the electron number N, and its inverse, softness, provide crucial information about the system's response to external perturbations [22]-[24].

$$\eta=\left(\frac{\partial\mu}{\partial N}\right)_{V(r)}=\left(\frac{\partial^2E}{\partial N^2}\right)_{V(r)}=\frac{1}{S}$$

Incorporating these descriptors into our analysis allows for a deeper understanding and prediction of the physicochemical properties of the studied *N-acylhydrazones*, thereby offering avenues for the design and optimization of more efficient compounds.

Drawing on Pearson's theory of acids and bases, [25] hardness (η) and softness (S) can be expressed in terms of ionization potentials (PI) and electron affinity (AE) as follows:

$$\eta=\frac{1}{S}=\left(\mathrm{PI}-\mathrm{AE}\right)/2$$

Ionization potential (PI) and electron affinity (AE) can be readily determined using the Koopmans approximation [26].

$$\mathrm{PI}=-\mathcal{E}_{\mathrm{HOMO}}\quad\text{and}\quad\mathrm{AE}=-\mathcal{E}_{\mathrm{LUMO}}$$

Here, $\mathcal{E}_{\text{HOMO}}$ and $\mathcal{E}_{\text{LUMO}}$ represent respectively the energies of the highest occupied orbital (HOMO) and the lowest unoccupied orbital (LUMO), respectively, in accordance with the theory of frontier molecular orbitals [27]. Furthermore, the energy gap ($\Delta\mathcal{E}$) serves as a crucial stability index, measuring a molecule's excitability. A reduced energy gap signifies heightened interaction with the environment, implying greater reactivity. Conversely, a larger gap between HOMO and LUMO energies indicates higher stability, thereby reducing the molecule's reactivity in chemical reactions.

$$\Delta\mathcal{E} = \mathcal{E}_{\text{LUMO}} - \mathcal{E}_{\text{HOMO}}$$

3) Local and dual descriptors

In 2004, Morell *et al*. [28] introduced a groundbreaking reactivity descriptor, known as the "dual descriptor", offering a novel approach on characterizing reactive sites within a molecule. This descriptor, defined as the difference between the Fukui functions (f_k^+ and f_k^-) for nucleophilic and electrophilic attacks, respectively, provides valuable insights into the reactivity of molecular sites. The value of the dual descriptor is calculated as follows:

$$f_k^+ = q_k(N+1) - q_k(N) \text{ et } f_k^- = q_k(N) - q_k(N-1)$$

$$\Delta f(r) = f_k^+ - f_k^-$$

f_k^+ for nucleophilic attack;

f_k^- for electrophilic attack;

$q_k(N)$ Electronic population of atom k in the neutral molecule;

$q_k(N+1)$ Electronic population of atom k in the anionic molecule;

$q_k(N-1)$ Electronic population of atom k in the cationic molecule.

When $\Delta f(r) > 0$, the region is identified as electrophilic, indicating a propensity for nucleophilic attack. Conversely, when $\Delta f(r) < 0$, the region is deemed nucleophilic, suggesting a predilection for electrophilic attack.

This method offers a robust approach to pinpointing and characterizing reactive sites in a molecule, thereby enhancing our ability to comprehend and predict chemical interactions. By integrating the dual descriptor into our analysis, we can delve deeper into molecular reactivity mechanisms, thereby unlocking novel avenues for the design and optimization of compounds with desired chemical properties. The introduction of the "dual descriptor" index presents a significant advancement, allowing for the simultaneous detection of both electrophilic and nucleophilic regions within a molecule. By examining a given region's dual descriptor, we can discern its preference for either nucleophilic or electrophilic attack.

4) The Hirshfeld populations

Incorporating Hirshfeld population analysis into our research promises a comprehensive characterization of molecular reactivity properties, thereby advancing our understanding of chemical mechanisms and facilitating the rational design of novel compounds with optimized chemical attributes. Hirshfeld charges provide a qualitative perspective align with fundamental chemical principles, affording a

means to quantify the electrophilicity and nucleophilicity of molecular surfaces [29] [30]. This method relies on an intuitive approach wherein the charge density at each point of the molecule is distributed among its constituent atoms, proportionally to their respective free atomic densities at the corresponding distances from the nucleus [31]. In this study, atomic charge values were determined via Hirshfeld population analysis, renowned for its robustness and capacity to furnish intricate insights into charge distribution within molecules. Through the quantification of atomic charges, we gain the ability to pinpoint electrophilic and nucleophilic regions within the molecule, offering invaluable insights into potential reactive sites. This analytical framework could promise for advancing our understanding of molecular reactivity and guiding the strategic design of compounds with tailored chemical properties.

3. Results and Discussion

As shown in **Figure 2**, we adopted this general numbering of imidazo [1,2-a] pyridine *N-acylhydrazones* derivatives to facilitate interpretation of the results.

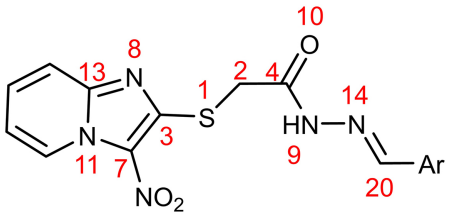

Figure 2. Numbered basic structure of imidazo [1,2-a] pyridine *N-acylhydrazones*.

3.1. Global Reactivity

For each compound, the energies of the Highest Occupied Molecular Orbital (HOMO) and Lowest Unoccupied Molecular Orbital (LUMO) orbitals provide vital insights into its stability and reactivity. A high HOMO energy signifies an enhanced ability to accept electrons, whereas a low LUMO energy indicates a predisposition to donate electrons. The evaluation of hardness (η) and softness (S) allows for the assessment of global reactivity, with higher hardness associated with lower reactivity and vice versa. These reactivity parameters offer a comprehensive overview of the physicochemical properties of the compounds under investigation, furnishing valuable insights into their behavior in reaction contexts and their potential applications across various domains of chemistry and pharmacology. The reactivity parameters examined in this series of compounds encompass HOMO energies ($\mathcal{E}_{\text{HOMO}}$), LUMO energies ($\mathcal{E}_{\text{LUMO}}$), hardness ($\eta$), softness ($S$), and the energy gap between the boundary orbitals ($\Delta\mathcal{E}$). The calculated values of these parameters are presented in **Table 2**.

The energy gap between the frontier orbitals ($\Delta\mathcal{E}$) serves as a pivotal indicator of molecular stability and reactivity: a larger $\Delta\mathcal{E}$ signifies lower reactivity and heightened stability, whereas a diminished $\Delta\mathcal{E}$ suggests increased reactivi-

ty. Analysis of the data presented in Table 2 reveals a range of $\Delta\mathcal{E}$ values spanning from 2.49 eV to 3.91 eV among the studied compounds. Notably, a smaller energy gap indicates a greater likelihood of electron transfer from the Highest Occupied Molecular Orbital (HOMO) to the Lowest Unoccupied Molecular Orbital (LUMO), indicative of heightened reactivity. Among the examined molecules, **9e** exhibits the largest energy gap (3.91 eV), signifying its superior stability and reduced reactivity. Conversely, **9j** displays the smallest energy gap (2.49 eV), rendering it the least stable yet most reactive compound in the series. By ranking the compounds based on stability, we obtain the following order:

Table 2. Energies of HOMO and LUMO frontier orbitals, hardness, softness (eV) −1, and energy gap. The other parameters are expressed in eV.

Compounds	$\mathcal{E}_{\text{HOMO}}$	$\mathcal{E}_{\text{LUMO}}$	$\Delta\mathcal{E}$	η	S
9a	−6.36	−2.89	3.47	1.74	0.58
9b	−6.10	−2.84	3.26	1.63	0.61
9c	−6.41	−2.93	3.48	1.74	0.57
9d	−6.19	−2.87	3.32	1.66	0.60
9e	−7.00	−3.09	**3.91**	**1.96**	0.51
9f	−6.20	−2.86	3.34	1.67	0.60
9g	−5.87	−2.85	3.02	1.51	0.66
9h	−6.00	−2.87	3.13	1.56	0.64
9i	−6.81	−3.03	3.78	1.89	0.53
9j	−5.28	−2.78	**2.49**	**1.25**	0.80
9k	−6.43	−2.94	3.49	1.74	0.57
9m	−6.58	−2.98	3.60	1.80	0.56
9n	−5.92	−2.76	3.16	1.58	0.63
9o	−6.00	−2.88	3.12	1.56	0.64
9p	−5.83	−2.88	2.95	1.47	0.68
9q	−6.10	−2.89	3.21	1.61	0.62
9r	−6.01	−2.89	3.12	1.56	0.64

9j < 9p < 9g < 9o; 9r < 9h < 9n < 9q < 9b < 9d < 9f < 9a < 9c < 9k < 9m < 9i < 9e.

This correlation underscores the significance of the energy gap in predicting the chemical properties and stability of the studied compounds, thereby offering valuable insights for the design of molecules with tailored characteristics, particularly in drug design and catalysis.

Examining the hardness values (η) provided in Table 2, we observe variations ranging from 1.25 eV to 1.96 eV among the molecules studied. Notably, lower hardness values correspond to higher reactivity. For instance, molecule **9j** exhibits the lowest hardness value (1.25 eV), rendering it the most reactive compound in the series. Ranking the molecules based on hardness yields the follow-

ing order:

9j > 9p > 9g > 9o; 9r > 9h > 9n > 9q > 9b > 9d > 9f > 9a > 9c > 9k > 9m > 9i > 9e.

This order aligns with the ranking derived from the energy gap ($\Delta\mathcal{E}$), corroborating the coherence of our findings.

Softness values ($\mathcal{S}$), as reported in Table 2, range from 0.51 eV^{-1} to 0.80 eV^{-1}. Higher softness values indicate less stability and greater reactivity. Once again, classifying the molecules according to softness reaffirms their reactivity order:

9j > 9p > 9g > 9o; 9r > 9h > 9n > 9q > 9b > 9d > 9f > 9a > 9c > 9k > 9m > 9i > 9e.

These results underscore the coherence of the three descriptors ($\Delta\mathcal{E}$, hardness, and softness) in providing insights into the stability and reactivity of the studied molecules.

3.2. Local Reactivity

3.2.1. Electrostatic Surface Potential Map

To gain insight into the electrophilic and nucleophilic sites within the compounds, an analysis of the electrostatic potential map was conducted, as depicted in Figure 3. In this analysis, negative regions (colored red or yellow) denote nucleophilic sites, whereas positive regions (colored cyan or blue) are indicative of electrophilic sites. This examination allows for a comprehensive understanding of the distribution of electrophilic and nucleophilic character within the compounds.

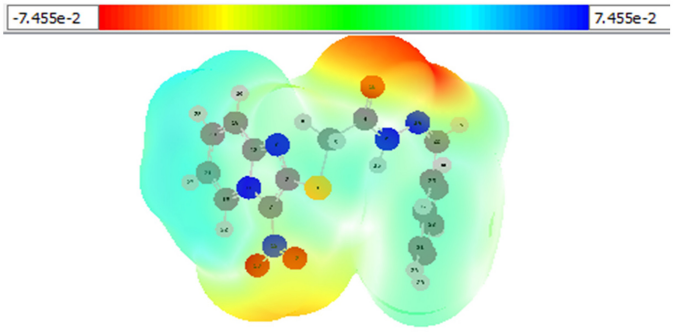

(**9a**)

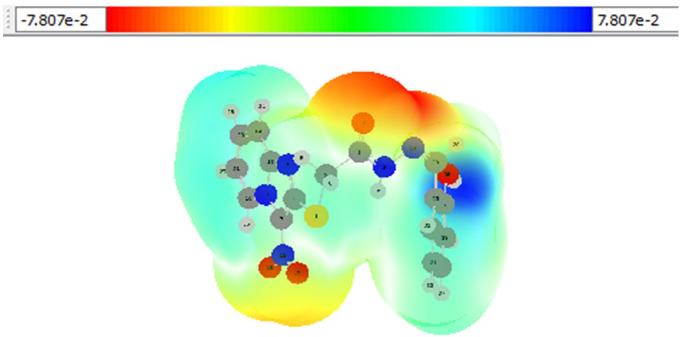

(**9b**)

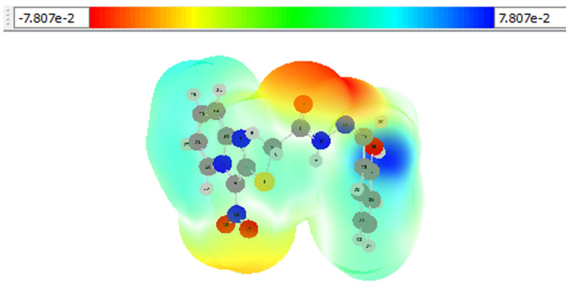
-7.807e-2
7.807e-2

(**9c**)

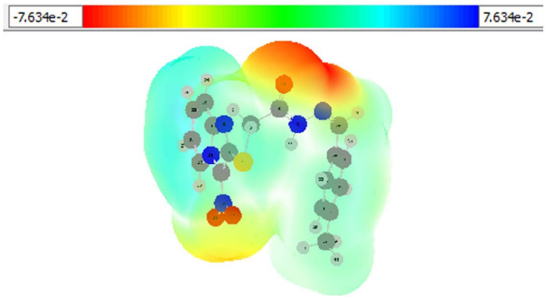
-7.634e-2
7.634e-2

(**9d**)

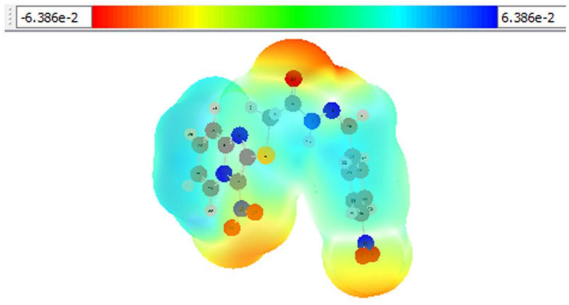
-6.386e-2
6.386e-2

(**9e**)

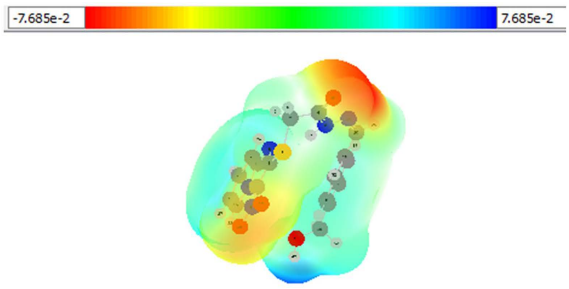
-7.685e-2
7.685e-2

(**9f**)

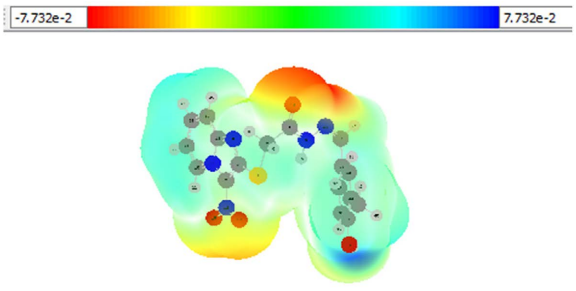
-7.732e-2
7.732e-2

(**9g**)

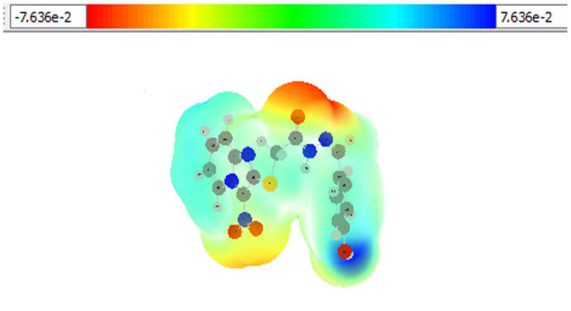
-7.636e-2
7.636e-2

(**9h**)

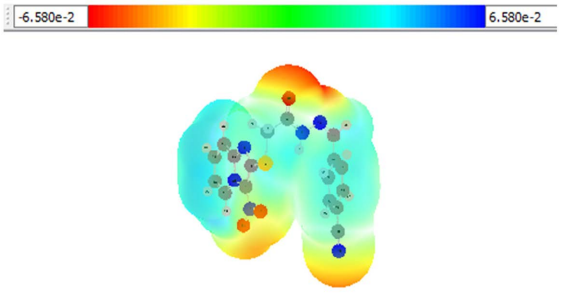
-6.580e-2
6.580e-2

(**9i**)

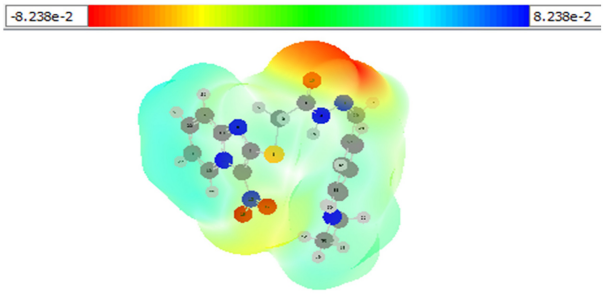
-8.238e-2
8.238e-2

(**9j**)

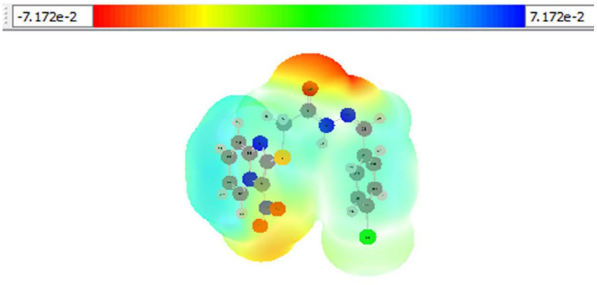
-7.172e-2
7.172e-2

(**9k**)

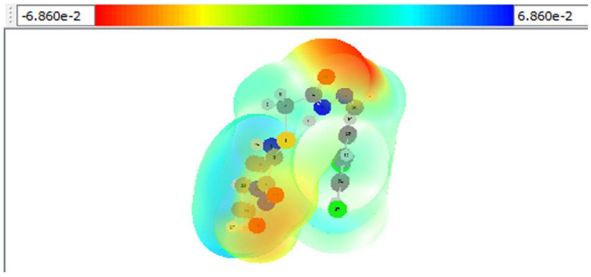
-6.860e-2
6.860e-2

(**9m**)

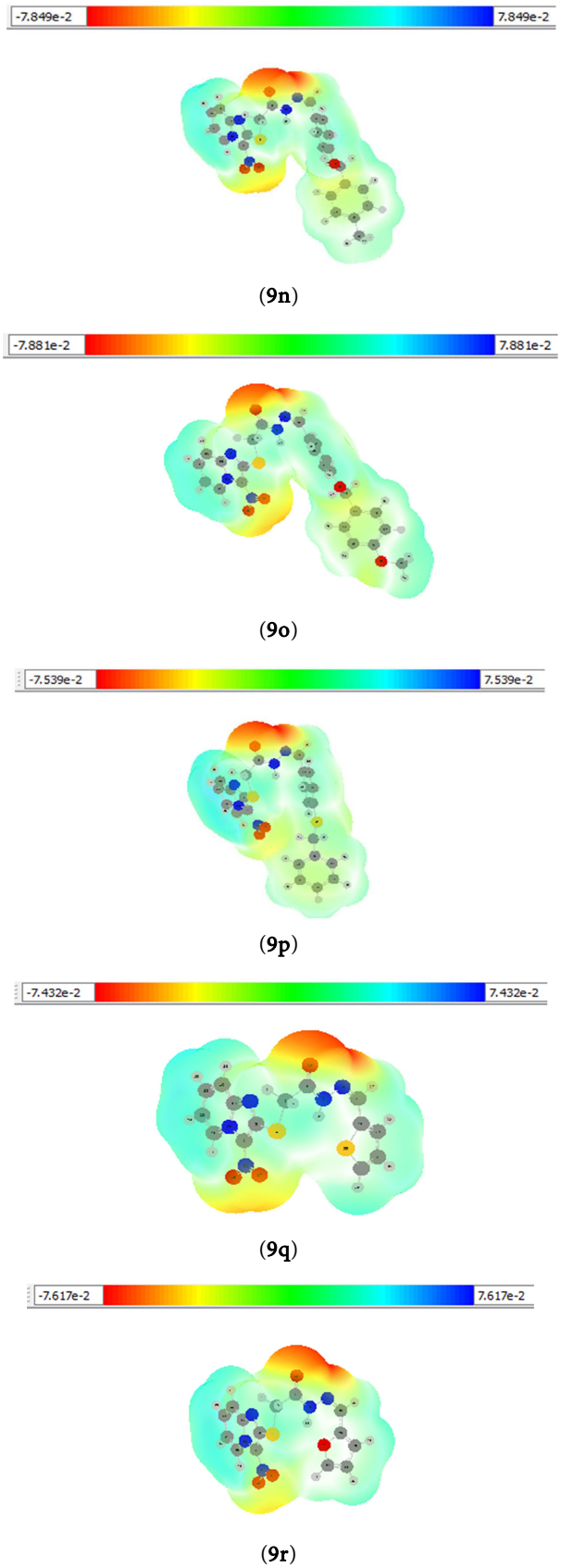

Figure 3. Map of the electrostatic potential of *N-acylhydrazones.*

Analysis of the electrostatic potential maps reveals distinct nucleophilic and electrophilic sites within the *N-acylhydrazones* under study. Specifically, the N9 and N14 nitrogen atoms, along with the O10 oxygen atom, exhibit nucleophilic character, making them favorable targets for electrophilic attack. In contrast, the N8 and N11 nitrogen atoms emerge as electrophilic sites, poised for nucleophilic interaction. Additionally, the S1 sulfur atom displays a discernible electrophilic tendency, due certainly to the lone pair electrons in its orbital. This meticulous examination of the electrostatic potential maps yields a comprehensive understanding of the reactive sites within each *N-acylhydrazone*. Such insights are instrumental for predicting and elucidating chemical reactions involving these compounds, thereby advancing our comprehension of their reactivity profiles.

3.2.2. Dual Descriptors

The values of the various dual descriptors are given in the following tables:

The comprehensive analysis of the dual descriptor values, outlined in Table 3 and Table s1-s16 (Tables s1-s16 in Supplemental material), unveils pivotal insights into the reactivity profiles of various reactive sites within the *N-acylhydrazone* molecules. In the case of the reference molecule **9a**, barring the nitro group, all heteroatoms exhibit nucleophilic character, rendering them susceptible to electrophilic attack. For molecules **9b**, **9c**, **9d**, **9f**, **9h**, **9i**, **9k**, **9q**, and **9r**, modification on the aryl ring at positions 2 or 4 imparts an electrophilic nature to nitrogens N8 and N11, thus facilitating nucleophilic attack. Conversely, nitrogens N9 and N14, oxygen O10, and sulfur S1 manifest nucleophilic behavior, promoting electrophilic attack.

Table 3. Local reactivity descriptors for **9a** using Hirschfeld charges at the theory 6-31+G(d,p) level.

ATOMS	$q_k(N)$	$q_k(N+1)$	$q_k(N-1)$	f_k^+	f_k^-	$\Delta f(r)$
1	7.973	7.922	7.948	−0.051	0.026	**−0.077**
2	3.029	3.022	3.026	−0.007	0.004	−0.011
3	2.980	2.978	2.979	−0.002	0.001	−0.003
4	2.907	2.893	2.900	−0.014	0.007	−0.021
7	2.973	2.959	2.966	−0.014	0.007	−0.021
8	3.608	3.605	3.607	−0.004	0.002	**−0.005**
9	3.529	3.503	3.516	−0.026	0.013	**−0.039**
10	4.154	4.106	4.130	−0.047	0.024	**−0.071**
11	3.502	3.497	3.499	−0.005	0.003	**−0.008**
13	2.941	2.935	2.938	−0.006	0.003	−0.009
14	3.557	3.534	3.545	−0.024	0.012	**−0.035**
20	2.985	2.957	2.971	−0.028	0.014	−0,042

In molecule **9e**, the introduction of a nitro group on the aryl ring at position 4 confers nucleophilic character to nitrogen N11, fostering electrophilic attack.

Meanwhile, nitrogen N14 exhibits a preference for nucleophilic attack, with negligible changes observed in the remaining heteroatoms. For molecules **9g**, **9j**, **9n**, **9o**, and **9p**, modification of the aryl ring at positions 3 and 4 or solely at position 4 induces an electrophilic character in nitrogens N8 and N11, as well as oxygen O10, promoting nucleophilic attack. Nitrogens N9 and N14, conversely, become more prone to electrophilic attack. Furthermore, the sulfur atom demonstrates electrophilic tendencies, further facilitating nucleophilic attack. In the case of molecule **9m**, chlorination of the aryl ring at positions 3 and 5 imparts nucleophilic character to all heteroatoms, except nitrogen N11, thereby promoting electrophilic attack. These detailed observations underscore the intricacies of molecular reactivity and emphasize the significance of analyzing the dual descriptor to characterize reactive sites within the studied compounds.

4. Conclusion

This theoretical investigation delves into seventeen *N-acylhydrazones*, shedding light on their reactivity and stability. Among these, molecule **9e** emerges as a standout, exhibiting distinct stability characteristics indicative of heightened resistance to electron transfer, as discerned through comprehensive analysis of global reactivity descriptors. By scrutinizing the electrostatic potential (ESP) maps and employing the dual descriptor, we pinpoint potential attack sites within the molecules. Notably, nitrogen atoms N9 and N14, along with oxygen O10, emerge as nucleophilic sites, while N8 and N11 nitrogen atoms generally exhibit electrophilic tendencies. Additionally, the sulfur atom displays a predisposition towards electrophilic attack. This study furnishes fundamental insights into the molecular reactivity of imidazo [1,2-a] pyridine *N-acylhydrazones*, with broad implications across diverse realms of chemistry, including drug design and catalysis. The acquired knowledge could serve as a springboard for future investigations aimed at the strategic design of compounds with tailored properties, geared towards pharmacomodulation.

Supplemental Material

Supplementary information for this article is provided in the online supplement.

Conflicts of Interest

The authors declare no conflicts of interest regarding the publication of this paper.

References

[1] Rozada, A.M., Rodrigues, F.A., Sampiron, E.G., Seixas, F.A., Basso, E.A., Scodro, R.B., *et al.* (2019) Novel 4-Methoxynaphthalene-*n-Acylhydrazone*s as Potential for Paracoccidioidomycosis and Tuberculosis Co-Infection. *Future Microbiology*, **14**, 587-598. https://doi.org/10.2217/fmb-2018-0357

[2] Velezheva, V., Brennan, P., Ivanov, P., Kornienko, A., Lyubimov, S., Kazarian, K., *et al.* (2016) Synthesis and Antituberculosis Activity of Indole-Pyridine Derived Hydrazides,

Hydrazide-Hydrazones, and Thiosemicarbazones. *Bioorganic & Medicinal Chemistry Letters*, **26**, 978-985. https://doi.org/10.1016/j.bmcl.2015.12.049

[3] De Miranda, A., Júnior, W., Da Silva, Y., Alexandre-Moreira, M., Castro, R., Sabino, J., *et al*. (2012) Design, Synthesis, Antinociceptive and Anti-Inflammatory Activities of Novel Piroxicam Analogues. *Molecules*, **17**, 14126-14145. https://doi.org/10.3390/molecules171214126

[4] Morjan, R.Y., Mkadmh, A.M., Beadham, I., Elmanama, A.A., Mattar, M.R., *et al*. (2014) Antibacterial Activities of Novel Nicotinic Acid Hydrazides and Their Conversion into N-acetyl-1,3,4-oxadiazoles. *Bioorganic & Medicinal Chemistry Letters*, **24**, 5796-5800.

[5] Ajani, O.O., Iyaye, K.T., Audu, O.Y., Olorunshola, S.J., Kuye, A.O. and Olanrewaju, I.O. (2018) Microwave Assisted Synthesis and Antimicrobial Potential of Quinoline-Based 4-Hydrazide-Hydrazone Derivatives. *Journal of Heterocyclic Chemistry*, **55**, 302-312.

[6] Rohane, S.H., Chauhan, A.J., Fuloria, N.K. and Fuloria, S. (2020) Synthesis and *in Vitro* Antimycobacterial Potential of Novel Hydrazones of Eugenol. *Arabian Journal of Chemistry*, **13**, 4495-4504. https://doi.org/10.1016/j.arabjc.2019.09.004

[7] Chezal, J., Paeshuyse, J., Gaumet, V., Canitrot, D., Maisonial, A., Lartigue, C., *et al*. (2010) Synthesis and Antiviral Activity of an Imidazo[1,2-A]pyrrolo[2,3-C]pyridine Series against the Bovine Viral Diarrhea Virus. *European Journal of Medicinal Chemistry*, **45**, 2044-2047. https://doi.org/10.1016/j.ejmech.2010.01.023

[8] Chitti, S., Singireddi, S., Santosh Kumar Reddy, P., Trivedi, P., Bobde, Y., Kumar, C., *et al*. (2019) Design, Synthesis and Biological Evaluation of 2-(3,4-Dimethoxyphenyl)-6 (1,2,3,6-Tetrahydropyridin-4-Yl)imidazo[1,2-A]pyridine Analogues as Antiproliferative Agents. *Bioorganic & Medicinal Chemistry Letters*, **29**, 2551-2558. https://doi.org/10.1016/j.bmcl.2019.08.013

[9] Nasr, T., Bondock, S. and Youns, M. (2014) Anticancer Activity of New Coumarin Substituted Hydrazide-Hydrazone Derivatives. *European Journal of Medicinal Chemistry*, **76**, 539-548.

[10] Morcoss, M., Abdelhafez, E.S., Abdel-Rahman, H., Abdel-Aziz, M. and Abou El-Ella, D. (2020) Novel Benzimidazole/Hydrazone Derivatives as Promising Anticancer Lead Compounds: Design, Synthesis, and Molecular Docking Study. *Journal of Advanced Biomedical and Pharmaceutical Sciences*, **3**, 45-52.

[11] Cikla, P., Küçükgüzel, G., Küçükgüzel, İ., Rollas, S., De Clercq, E., Pannecouque, C., *et al*. (2010) Synthesis and Evaluation of Antiviral, Antitubercular and Anticancer Activities of Some Novel Thioureas Derived from 4-Aminobenzohydrazide Hydrazones. *Marmara Pharmaceutical Journal*, **14**, 13-20.

[12] Reddy Gangireddy, M., Mantipally, M., Gundla, R., Nayak Badavath, V., Paidikondala, K. and Yamala, A. (2019) Design and Synthesis of Piperazine-Linked Imidazo[1,2-*a*]pyridine Derivatives as Potent Anticancer Agents. *ChemistrySelect*, **4**, 13622-13629. https://doi.org/10.1002/slct.201902955

[13] Şenkardeş, S., Kaushik-Basu, N., Durmaz, İ., Manvar, D., Basu, A., Atalay, R., *et al*. (2016) Synthesis of Novel Diflunisal Hydrazide-Hydrazones as Anti-Hepatitis C Virus Agents and Hepatocellular Carcinoma Inhibitors. *European Journal of Medicinal Chemistry*, **108**, 301-308. https://doi.org/10.1016/j.ejmech.2015.10.041

[14] Ablo, E., Coulibaly, S., Coulibali, S., Signo, K., Achi, P., Giraud, N., *et al*. (2022) Synthesis and Characterization of Novel Conformers of (*e*)-2-(3-nitro-*h*-imidazo[1,2-*a*]pyridin-2-ylthio)-*n*'-benzylideneacetohydrazide Derivatives. *Magnetic Resonance in Chemistry*, **60**, 1157-1170. https://doi.org/10.1002/mrc.5308

[15] Frisch, M.J., Trucks, G.W., Schlegel, H.B., Scuseria, G.E., Robb, M.A., Cheeseman,

J.R., *et al*. (2009) Gaussian 09, Revision, A.1. Gaussian Inc.

[16] Hohenberg, P. and Kohn, W. (1964) Inhomogeneous Electron Gas. *Physical Review*, **136**, B864-B871. https://doi.org/10.1103/physrev.136.b864

[17] Dennington, R., Keith, T. and Millam, J. (2009) GaussView, Version 5. Semichem Inc.

[18] Koch, W. and Holthausen, M.C. (2001) A Chemist's Guide to Density Functional Theory. 2nd Edition, Wiley.

[19] N'dri, J., Koné, M., Kodjo, C., kablan, A., Affi, S., Ouattara, L., *et al*. (2018) Theoretical Study of the Chemical Reactivity of Five Schiff Bases Derived from Dapsone by the DFT Method. *Chemical Science International Journal*, **22**, 1-11. https://doi.org/10.9734/csji/2018/41427

[20] Hirshfeld, F.L. (1977) Bonded-Atom Fragments for Describing Molecular Charge Densities. *Theoretica Chimica Acta*, **44**, 129-138. https://doi.org/10.1007/bf00549096

[21] Labet, V. (2009) Etude Théorique de Quelques Aspects de La Réactivité Des Bases de l'ADN-Définition de Nouveaux Outils Théoriques d'étude de La Réactivité Chimique. Thèse de doctorat, Université Joseph-Fourier-Grenoble.

[22] Sanderson, R.T. (1951) An Interpretation of Bond Lengths and a Classification of Bonds. *Science*, **114**, 670-672. https://doi.org/10.1126/science.114.2973.670

[23] Parr, R.G. and Pearson, R.G. (1983) Absolute Hardness: Companion Parameter to Absolute Electronegativity. *Journal of the American Chemical Society*, **105**, 7512-7516. https://doi.org/10.1021/ja00364a005

[24] Yang, W. and Parr, R.G. (1985) Hardness, Softness, and the Fukui Function in the Electronic Theory of Metals and Catalysis. *Proceedings of the National Academy of Sciences of the United States of America*, **82**, 6723-6726.

[25] Pearson, R.G. (1963) Hard and Soft Acids and Bases. *Journal of the American Chemical Society*, **85**, 3533-3539. https://doi.org/10.1021/ja00905a001

[26] Koopmans, T. (1934) Über die Zuordnung von Wellenfunktionen und Eigenwerten zu den Einzelnen Elektronen Eines Atoms. *Physica*, **1**, 104-113. https://doi.org/10.1016/s0031-8914(34)90011-2

[27] Fukui, K., Yonezawa, T. and Shingu, H. (1952) A Molecular Orbital Theory of Reactivity in Aromatic Hydrocarbons. *The Journal of Chemical Physics*, **20**, 722-725. https://doi.org/10.1063/1.1700523

[28] Morell, C., Grand, A. and Toro-Labbé, A. (2005) New Dual Descriptor for Chemical Reactivity. *The Journal of Physical Chemistry A*, **109**, 205-212.

[29] Wang, B., Rong, C., Chattaraj, P.K. and Liu, S. (2019) A Comparative Study to Predict Regioselectivity, Electrophilicity and Nucleophilicity with Fukui Function and Hirshfeld Charge. *Theoretical Chemistry Accounts*, **138**, Article No. 124. https://doi.org/10.1007/s00214-019-2515-1

[30] Stalke, D. (2011) Meaningful Structural Descriptors from Charge Density. *Chemistry—A European Journal*, **17**, 9264-9278.

[31] Tuo, N.T., Dembele, G.S., Doh, S., Konate, F., Konate, B., Kodjo, C.G., *et al*. (2022) Theoretical Study of the Chemical Reactivity of a Series of 2,3-Dihydro-1h-perimidine. *International Research Journal of Pure and Applied Chemistry*, **23**, 13-25. https://doi.org/10.9734/irjpac/2022/v23i130451

Supplemental Material

Procedure for the synthesis of *N-acylhydrazones* (9a-r)

1.23 mmol of 2-(1.8a-dihydro-3-nitroimidazo [1.2-a] pyridin-2-ylthio) acetohydrazide and 1.23 mmol (1 eq) of benzaldehyde derivative were dissolved in methanol. The reaction mixture was refluxed for 1 h. After cooling to room temperature, the precipitate formed was filtered, dried and then purified by recrystallization in a water/ethanol mixture (1/1) to give 2-(1.8a-dihydro-3-nitroimidazo [1.2-a] pyridin-2-ylthio)-N'-benzylideneacetohydrazide with yields between 56% and 86%.

(E)-2-(3-nitro-H-imidazo[1.2-a]pyridin-2-ylthio)-N'-benzylideneacetohydrazide (9a)

Orange powder. M.p = 232 - 234˚C; Yield = 79 %, ^{1}H NMR (300 MHz, DMSO -*d*6) δ (ppm) 11.77_{ap}, 11.67_{sp} (s, 1H; NH), $9.34_{(sp+ap)}$ (dt.*J* = 6.9, 1.1 *Hz*, 1H; H_{Ar}), 8.22_{ap}, 8.05_{sp} (s, 1H; N=CH), 7.90 – $7.77_{(sp+ap)}$ (m, 2H; H_{Ar}), $7.71_{(sp+ap)}$ (td, *J* = 3.8; 2.2 *Hz*, 2H; HAr), 7.51 – $7.34_{(sp+ap)}$ (m, 4H; H_{Ar}), 4.63_{sp}, 4.22_{ap} (s, 2H, S-CH_2). ^{13}C NMR (75 MHz, DMSO-*d*6) δ (ppm) 169.39_{sp}, 164.18_{ap} (C=O), 153.54_{sp}, 153.15_{ap} (N=CH), 147.44, 146.23, 144.16, 134.53, 134.48, 133.52_{sp}, 133.46_{ap} (C_{Ar}), 130.60_{sp}, 130.44_{ap} (C_{Ar}), 129.29, 128.65_{sp}, 128.40_{ap} (C_{Ar}), 127.58, 127.34, 11697_{sp}, 116.87_{ap} (C_{Ar}), 116.79, 33.95_{ap}, 33.08_{sp} (S-CH_2), HRMS (ESI):Calc for [M+Na^+] $C_{16}H_{13}N_5NaO_3S$ = 378.0521. Found = 378.0525.

^{1}H and ^{13}C NMR spectra of 2-(3-nitro-*H*-imidazo [1.2-a] pyridin-2-ylthio)-N'-benzylideneacetohydrazide (9a)

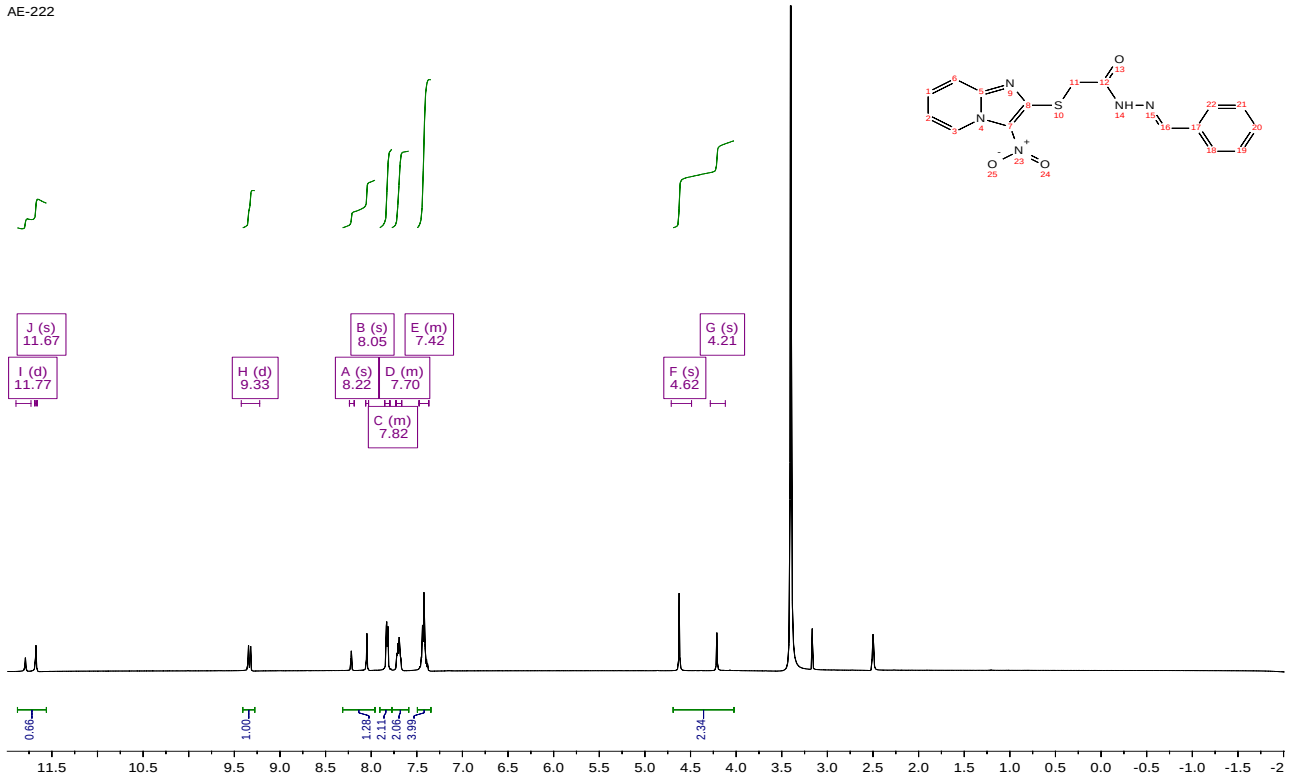

Figure S1. ^{1}H NMR spectra.

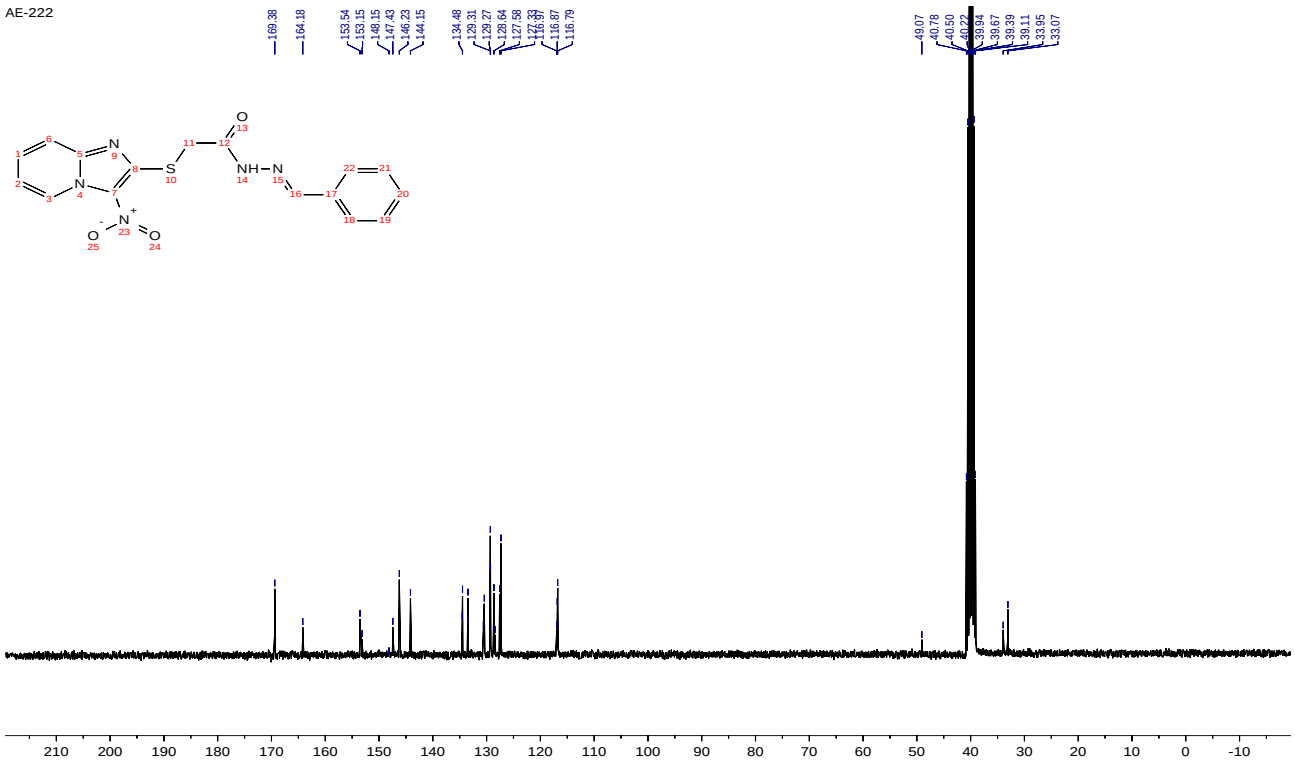

Figure S2. ^{13}C NMR spectra.

Table S1. Local reactivity descriptors for **9b** using Hirschfeld charges at the theory 6-31+G(d,p) level.

ATOMS	$q_k(N)$ (N)	$q_k(N+1)$ (N + 1)	$q_k(N-1)$ (N − 1)	f_k^+	f_k^-	$\Delta f(r)$
1	7.974	7.931	8.002	−0.043	−0.028	**−0.015**
2	3.029	3.023	3.036	−0.006	−0.007	0.001
3	2.980	2.978	2.998	−0.001	−0.019	0.018
4	2.908	2.895	2.910	−0.013	−0.002	−0.011
7	2.973	2.961	2.979	−0.012	−0.006	−0.006
8	3.608	3.605	3.623	−0.002	−0.016	**0.013**
9	3.530	3.507	3.529	−0.023	0.001	**−0.024**
10	4.154	4.112	4.168	−0.043	−0.014	**−0.029**
11	3.502	3.498	3.512	−0.004	−0.010	**0.006**
13	2.941	2.936	2.961	−0.005	−0.020	0.015
14	3.557	3.533	3.564	−0.024	−0.007	**−0.017**
20	2.984	2962	2.994	−0.022	−0.010	−0.013

Table S2. Local reactivity descriptors for **9C** using Hirschfeld charges at the theory 6-31+G(d,p) level.

ATOMS	$q_k(N)$ (N)	$q_k(N+1)$ (N + 1)	$q_k(N-1)$ (N − 1)	f_k^+	f_k^-	$\Delta f(r)$
1	7.974	7.923	8.001	−0.050	−0.027	**−0.023**
2	3.029	3.022	3.036	−0.007	−0.007	0.000
3	2.980	2.978	2.999	−0.002	−0.019	0,017

Continued

4	2.907	2.893	2.909	−0.014	−0.003	−0.011
7	2.973	2.959	2.979	−0.015	−0.006	−0.009
8	3.609	3.605	3.624	−0.003	−0.016	0.012
9	3.529	3.504	3.529	−0.025	0.001	**−0.026**
10	4.153	4.107	4.168	−0.046	−0.015	**−0.031**
11	3.502	3.497	3.512	−0.005	−0.010	**0.005**
13	2.941	2.935	2.961	−0.006	−0.020	0.014
14	3.557	3.534	3.566	−0.023	−0,009	**−0.015**
20	2.985	2.959	2.996	−0.026	−0.011	−0.016

Table S3. Local reactivity descriptors for **9d** using Hirschfeld charges at the theory 6-31+G(d,p) level.

ATOMS	$q_k(N)$ (N)	$q_k(N+1)$ (N + 1)	$q_k(N-1)$ (N − 1)	f_k^+	f_k^-	$\Delta f(r)$
1	7.973	7.930	8.002	−0.043	−0.029	**−0.013**
2	3.029	3.023	3.036	−0.006	−0.007	0.001
3	2.980	2.979	3.000	−0.001	−0.020	0.020
4	2.907	2.893	2.909	−0.014	−0.002	−0.012
7	2.973	2.964	2.979	−0.010	−0.006	−0.004
8	3.608	3.605	3.625	−0.003	−0.017	0.014
9	3.530	3.503	3.528	−0.027	0.001	**−0.028**
10	4.154	4.109	4.168	−0.046	−0.014	**−0.032**
11	3.502	3.498	3.513	−0.004	−0.011	**0.007**
13	2.941	2.936	2.962	−0.005	−0.021	0.017
14	3.558	3.532	3.564	−0.026	−0.006	**−0.021**
20	2.985	2.958	2.993	−0.027	−0.008	−0.018

Table S4. Local reactivity descriptors for **9e** using Hirschfeld charges at the theory 6-31+G(d,p) level.

ATOMS	$q_k(N)$ (N)	$q_k(N+1)$ (N + 1)	$q_k(N-1)$ (N − 1)	f_k^+	f_k^-	$\Delta f(r)$
1	7.974	7.911	7.987	−0.062	−0.014	**−0.048**
2	3.029	3.020	3.034	−0.009	−0.005	−0.004
3	2.981	2.976	2.989	−0.005	−0.008	0.003
4	2.905	2.893	2.910	−0.012	−0.005	−0.007
7	2.973	2.950	2.976	−0.024	−0.002	−0.022
8	3.609	3.603	3.616	−0.006	−0.007	0.002
9	3.528	3.508	3.530	−0.021	−0.002	**−0.019**
10	4.148	4.104	4.165	−0.045	−0.017	**−0.028**
11	3.502	3.496	3.507	−0.006	−0.005	**−0.001**
13	2.941	2.932	2.951	−0.009	−0.010	0.002
14	3.552	3.535	3.571	−0.016	−0.019	**0.003**
20	2.985	2.960	2.995	−0.026	−0.009	−0.016

Table S5. Local reactivity descriptors for **9f** using Hirschfeld charges at the theory 6-31+G(d,p) level.

ATOMS	$q_k(N)$ (N)	$q_k(N+1)$ (N + 1)	$q_k(N-1)$ (N − 1)	f_k^+	f_k^-	$\Delta f(r)$
1	7.970	7.914	8.000	−0.057	−0.030	**−0.027**
2	3.029	3.022	3.036	−0.007	−0.008	0.001
3	2.980	2.980	2.998	0.000	−0.018	0.018
4	2.909	2.895	2.913	−0.014	−0.004	−0.010
7	2.973	2.961	2.978	−0.012	−0.006	−0.006
8	3.607	3.607	3.621	0.000	−0.014	**0.014**
9	3.530	3.498	3.529	−0.033	0.001	**−0.033**
10	4.153	4.108	4.169	−0.045	−0.017	**−0.028**
11	3.500	3.496	3.510	−0.004	−0.011	**0.007**
13	2.941	2.938	2.960	−0.003	−0.019	0.016
14	3.558	3.532	3.568	−0.026	−0.009	**−0.017**
20	2.985	2.954	2.995	−0.031	−0.010	−0.021

Table S6. Local reactivity descriptors for **9g** using Hirschfeld charges at the theory 6-31+G(d,p) level.

ATOMS	$q_k(N)$ (N)	$q_k(N+1)$ (N + 1)	$q_k(N-1)$ (N − 1)	f_k^+	f_k^-	$\Delta f(r)$
1	7.974	7.952	8.002	−0.022	−0.028	**0.007**
2	3.029	3.025	3.036	−0.004	−0.007	0.003
3	2.980	2.980	2.999	0.001	−0.020	0.020
4	2.908	2.896	2.909	−0.012	−0.001	−0.010
7	2.973	2.962	2.979	−0.011	−0.006	−0.005
8	3.607	3.606	3.624	−0.001	−0.017	**0.015**
9	3.530	3.506	3.529	−0.025	0.001	**−0.026**
10	4.154	4.119	4.167	−0.035	−0.013	**−0.022**
11	3.502	3.500	3.513	−0.002	−0.011	**0.009**
13	2.941	2.938	2.962	−0.003	−0.021	0.018
14	3.560	3.530	3.565	−0.030	−0.005	**−0.026**
20	2.986	2.963	2.995	−0.023	−0.009	−0.014

Table S7. Local reactivity descriptors for **9h** using Hirschfeld charges at the theory 6-31+G(d,p) level.

ATOMS	$q_k(N)$ (N)	$q_k(N+1)$ (N + 1)	$q_k(N-1)$ (N − 1)	f_k^+	f_k^-	$\Delta f(r)$
1	7.974	8.002	7942	0.028	0.032	**−0.004**
2	3.029	3.036	3.024	0.007	0.005	0.002
3	2.980	2.999	2.979	0.019	0.000	0.019
4	2.908	2.909	2.895	0.002	0.013	−0.011
7	2.973	2.979	2.964	0.006	0.010	−0.004
8	3.608	3.624	3.607	0.016	0.001	**0.015**

Continued

9	3.530	3.529	3.505	−0.001	0.025	**−0.026**
10	4.154	4.167	4.113	0.014	0.041	**−0.028**
11	3.502	3.513	3.498	0.011	0.004	**0.007**
13	2.941	2.962	2.937	0.021	0.004	0.017
14	3.560	3.565	3.531	0.006	0.029	**−0.023**
20	2.986	2.995	2.963	0.009	0.023	−0.014

Table S8. Local reactivity descriptors for **9i** using Hirschfeld charges at the theory 6-31+G(d,p) level.

ATOMS	$q_k(N)$ (N)	$q_k(N+1)$ (N + 1)	$q_k(N-1)$ (N − 1)	f_k^+	f_k^-	$\Delta f(r)$
1	7.973	7.916	7.993	−0.057	−0.020	**−0.037**
2	3.029	3.021	3.035	−0.008	−0.006	−0.002
3	2.981	2.977	2.993	−0.003	−0.012	0.009
4	2.905	2.892	2.911	−0.013	−0.006	−0.007
7	2.973	2.955	2.977	−0.018	−0.004	−0.014
8	3.609	3.604	3.620	−0.005	−0.011	**0.006**
9	3.528	3.505	3.529	−0.023	−0.001	**−0.021**
10	4.150	4.105	4.168	−0.044	−0.018	**−0.027**
11	3.502	3.496	3.509	−0.006	−0.007	**0.002**
13	2.941	2.934	2.956	−0.007	−0.014	0.007
14	3.553	3.534	3.571	−0.019	−0.018	**−0.001**
20	2.985	2.959	2.999	−0.026	−0.014	−0.012

Table S9. Local reactivity descriptors for **9j** using Hirschfeld charges at the theory 6-31+G(d,p) level.

ATOMS	$q_k(N)$ (N)	$q_k(N+1)$ (N + 1)	$q_k(N-1)$ (N − 1)	f_k^+	f_k^-	$\Delta f(r)$
1	7.972	7.966	8.003	−0.006	−0.031	**0.025**
2	3.029	3.026	3.037	−0.003	−0.007	0.004
3	2.979	2.981	3.000	0.002	−0.021	0.023
4	2.909	2.898	2.910	−0,011	−0.001	−0.009
7	2.973	2.974	2.978	0.001	−0.006	0.007
8	3.608	3.608	3.625	0.000	−0.017	**0.017**
9	3.530	3.512	3.528	−0.018	0.002	**−0.019**
10	4.157	4.127	4.171	−0.030	−0.014	**−0.015**
11	3.502	3.502	3.513	0.001	−0.011	**0.012**
13	2.940	2.940	2.962	−0.001	−0.022	0.021
14	3.564	3.530	3.568	−0.034	−0.004	**−0.029**
20	2.987	2.973	2.993	−0.014	−0.006	−0.008

Table S10. Local reactivity descriptors for **9k** using Hirschfeld charges at the theory 6-31+G(d,p) level.

ATOMS	$q_k(N)$ (N)	$q_k(N+1)$ (N + 1)	$q_k(N-1)$ (N − 1)	f_k^+	f_k^-	$\Delta f(r)$
1	7.973	7.925	7.999	−0.048	−0.026	**−0.022**
2	3.029	3.022	3.036	−0.007	−0.007	0.000
3	2.980	2.979	2.998	−0.002	−0.018	0.016
4	2.906	2.893	2.910	−0.013	−0.004	−0.010
7	2.973	2.961	2.979	−0.012	−0.005	−0.007
8	3.609	3.606	3.624	−0.004	−0.015	**0.011**
9	3.529	3.504	3.528	−0.025	0.000	**−0.025**
10	4.152	4.108	4.168	−0.044	−0.016	**−0.028**
11	3.502	3.497	3.511	−0.005	−0.010	**0.005**
13	2.941	2.935	2.960	−0.006	−0.019	0.013
14	3.556	3.533	3.567	−0.023	−0.011	**−0.012**
20	2.985	2.960	2.997	−0.026	−0.012	−0.014

Table S11. Local reactivity descriptors for **9m** using Hirschfeld charges at the theory 6-31+G(d,p) level.

ATOMS	$q_k(N)$ (N)	$q_k(N+1)$ (N + 1)	$q_k(N-1)$ (N − 1)	f_k^+	f_k^-	$\Delta f(r)$
1	7.968	7.896	7.995	−0.072	−0.027	**−0.045**
2	3.028	3.020	3.035	−0.008	−0.007	−0.001
3	2.980	2.978	2.995	−0.002	−0.015	0.013
4	2.907	2.895	2.918	−0.013	−0.011	−0.002
7	2.973	2.955	2.978	−0.018	−0.005	−0.013
8	3.608	3.605	3.300	−0.002	0.308	**−0.310**
9	3.530	3.502	3.530	−0.028	0.000	**−0.027**
10	4.149	4.105	4.167	−0.043	−0.018	**−0.025**
11	3.500	3.496	3.510	−0.005	−0.009	**0.004**
13	2.942	2.936	2.958	−0.006	−0.016	0.010
14	3.554	3.534	3.568	−0.019	−0.014	**−0.005**
20	2.985	2.955	2.998	−0.030	−0.013	−0.017

Table S12. Local reactivity descriptors for **9n** using Hirschfeld charges at the theory 6-31+G(d,p) level.

ATOMS	$q_k(N)$ (N)	$q_k(N+1)$ (N + 1)	$q_k(N-1)$ (N − 1)	f_k^+	f_k^-	$\Delta f(r)$
1	7.974	7.957	8.002	−0.017	−0.029	**0.011**
2	3.029	3.025	3.036	−0.004	−0.007	0.003
3	2.980	2.981	2.999	0.001	−0.020	0.021
4	2.908	2.897	2.909	−0.011	−0.001	−0.010
7	2.973	2.970	2.979	−0.004	−0.006	0.002
8	3.607	3.608	3.624	0.000	−0.017	**0.017**

Continued

9	3.530	3.508	3.529	−0.023	0.001	**−0.024**
10	4.155	4.120	4.167	−0.035	−0.013	**−0.022**
11	3.502	3.500	3.513	−0.002	−0.011	**0.009**
13	2.941	2.939	2.962	−0.002	−0.021	0.019
14	3.561	3.532	3.565	−0.028	−0.004	**−0.024**
20	2.986	2.966	2.994	−0.020	−0.009	−0.011

Table S13. Local reactivity descriptors for **9o** using Hirschfeld charges at the theory 6-31+G(d,p) level.

ATOMS	$q_k(N)$ (N)	$q_k(N+1)$ (N + 1)	$q_k(N-1)$ (N − 1)	f_k^+	f_k^-	$\Delta f(r)$
1	7.974	8.002	7.961	0.028	0.012	**0.016**
2	3.029	3.036	3.026	0.007	0.003	0.004
3	2.980	2.999	2.981	0.020	−0.001	0.021
4	2.908	2.909	2.898	0.001	0.010	−0.009
7	2.973	2.979	2.971	0.006	0.002	0.004
8	3.607	3.624	3.608	0.017	0.000	**0.017**
9	3.530	3.529	3.510	−0.001	0.020	**−0.021**
10	4.155	4.168	4.124	0.013	0.031	**−0.018**
11	3.502	3.513	3.501	0.011	0.001	**0.009**
13	2.941	2.962	2.939	0.021	0.002	0.020
14	3.561	3.565	3.536	0.004	0.025	**−0.021**
20	2.986	2.995	2.969	0.009	0.017	−0.009

Table S14. Local reactivity descriptors for **9p** using Hirschfeld charges at the theory 6-31+G(d,p) level.

ATOMS	$q_k(N)$ (N)	$q_k(N+1)$ (N + 1)	$q_k(N-1)$ (N − 1)	f_k^+	f_k^-	$\Delta f(r)$
1	7.972	8.002	7.962	0.031	0.010	**0.020**
2	3.029	3.036	3.025	0.007	0.003	0.004
3	2.979	3.000	2.980	0.021	−0.001	0.023
4	2.907	2.909	2.898	0.001	0.010	−0.009
7	2.972	2.978	2.972	0.006	0.000	0.006
8	3.608	3.625	3.607	0.017	0.001	**0.016**
9	3.530	3.528	3.512	−0.002	0.017	**−0.019**
10	4.155	4.169	4.125	0.014	0.030	**−0.016**
11	3.501	3.512	3.502	0.011	0.000	**0.011**
13	2.940	2.962	2.939	0.021	0.001	0.020
14	3.559	3.563	3.532	0.005	0.026	**−0.022**
20	2.985	2.992	2.970	0.007	0.015	−0.008

Table S15. Local reactivity descriptors for **9q** using Hirschfeld charges at the theory 6-31+G(d,p) level.

ATOMS	$q_k(N)$ (N)	$q_k(N+1)$ (N + 1)	$q_k(N-1)$ (N − 1)	f_k^+	f_k^-	$\Delta f(r)$
1	7.974	7.999	7.947	0.025	0.026	**−0.001**
2	3.029	3.036	3.024	0.007	0.005	0.002
3	2.980	2.996	2.980	0.016	0.000	0.016
4	2.906	2.910	2.894	0.004	0.012	−0.009
7	2.973	2.978	2.958	0.005	0.015	−0.010
8	3.608	3.622	3.605	0.014	0.003	**0.011**
9	3.529	3.529	3.502	0.000	0.027	**−0.028**
10	4.151	4.167	4.113	0.015	0.038	**−0.022**
11	3.502	3.511	3.499	0.009	0.003	**0.007**
13	2.941	2.959	2.937	0.018	0.004	0.014
14	3.560	3.571	3.528	0.011	0.032	**−0.020**
20	3.023	3.042	3.012	0.019	0.011	0.009

Table S16. Local reactivity descriptors for **9r** using Hirschfeld charges at the theory 6-31+G(d,p) level.

ATOMS	$q_k(N)$ (N)	$q_k(N+1)$ (N + 1)	$q_k(N-1)$ (N − 1)	f_k^+	f_k^-	$\Delta f(r)$
1	7.972	8.002	7.938	0.030	0.033	**−0.004**
2	3.029	3.036	3.023	0.007	0.006	0.002
3	2.979	2.998	2.979	0.020	0.000	0.020
4	2.908	2.910	2.893	0.002	0.014	−0.012
7	2.973	2.978	2.966	0.005	0.007	−0.001
8	3.607	3.623	3.604	0.016	0.003	**0.013**
9	3.530	3.528	3.500	−0.001	0.030	**−0.031**
10	4.154	4.169	4.110	0.015	0.044	**−0.029**
11	3.502	3.512	3.499	0.010	0.003	**0.007**
13	2.940	2.961	2.936	0.021	0.004	0.016
14	3.559	3.567	3.526	0.008	0.034	**−0.026**
20	3.023	3.044	3.009	0.021	0.013	0.008